CHEMISTRY OF MATERIALS
Article

Chem. Mater. **2009,** *21,* 3275–3281 3275
DOI:10.1021/cm900785u

Synthesis and Covalent Surface Functionalization of Nonoxidic Iron Core−Shell Nanomagnets

Inge K. Herrmann, Robert N. Grass, Dmitry Mazunin, and Wendelin J. Stark*

Institute for Chemical and Bioengineering, Department of Chemistry and Applied Biosciences, ETH Zurich, 8093 Zurich, Switzerland

Received March 20, 2009. Revised Manuscript Received May 12, 2009

The rapidly growing applications of nanomagnets require acid/base stable, oxidation-resistant shells with chemically controlled surface structure. An ideal core should be metallic and highly magnetic. We demonstrate the production of iron-based nanoparticles, ranging from iron oxide to iron and iron carbide, by systematically modifying the degree of reduction during flame spray synthesis under a controlled atmosphere. At a laboratory scale, continuous production yields iron-based particles of 20−50 nm at a production rate of >10 g h^{-1}. Carbon-encapsulated iron carbide (C/Fe_3C) combines exceptionally high saturation magnetization (140 emu g^{-1}), air stability (up to 200 °C), and resistance against acidic dissolution (1 week in 24% HCl). The top graphene-like carbon layer could be covalently functionalized with various linkers, thus allowing us to chemically design the particle surface. Activity was demonstrated by reacting 2-phenyl ethyl amine functionalized nanomagnets with carboxylic acid chlorides as a model reaction. The present nanomagnets consist of biologically well-accepted constituents. They combine the required chemical reliability, improved magnetization if compared to magnetite with the potential for technical scale manufacturing, and therefore open stable nanomagnets to a broad range of fascinating separation problems (extraction/water treatment) and biomedical research.

Introduction

Nanomagnets are of great interest for a wide variety of applications ranging from magnetic fluids,[1] data storage,[2] and environmental remediation[3] to medicinal imaging[4,5] and drug delivery.[6] A number of suitable methods has been developed for the synthesis of magnetic nanoparticles of different compositions and phases with distinct magnetic properties.[7] In principle, nanomagnets with the strongest magnetic properties for above applications could be obtained by the use of metals[8,9] (Co, Fe, saturation magnetization $M_{s,bulk} \leq 220$ emu g^{-1}) or metal alloys[10] (CoFe, CoNiFe, $M_{s,bulk} \leq 245$ emu g^{-1}). Unfortunately, naked metal nanoparticles are chemically highly active (typically pyrophoric) and readily oxidized upon contact with air,[9] generally resulting in loss of magnetism and dispersibility. Up to now, this has promoted the widespread use of moderately magnetic oxide nanoparticles, such as magnetite ($M_{s,bulk} \leq 92$ emu g^{-1}).[11−13]

Use of magnetic nanoparticles in the above-mentioned applications strongly depends on a rapid response of the nanomagnets to magnetic field gradients and additionally requires stability under a wide range of different conditions (acidic/basic media, sterilization, solvent compatibility, and high temperatures). Core−shell structured materials are therefore attracting increasing interest because they combine favorable properties of the magnetic (ideally metallic) core with a protective polymer,[14] silica[15] gold,[16,17] metal oxide,[18] or carbon[19] shell. It is noteworthy

*Corresponding author. E-mail: wendelin.stark@chem.ethz.ch. Phone: 41 44 632 09 80. Fax: 41 44 633 10 83.

(1) Shen, L. F.; Stachowiak, A.; Hatton, T. A.; Laibinis, P. E. *Langmuir* **2000**, *16*, 9907–9911.
(2) Hyeon, T. *Chem. Commun.* **2003**, 927–934.
(3) Elliott, D. W.; Zhang, W. X. *Environ. Sci. Technol.* **2001**, *35*, 4922–4926.
(4) Gao, J. H.; Liang, G. L.; Cheung, J. S.; Pan, Y.; Kuang, Y.; Zhao, F.; Zhang, B.; Zhang, X. X.; Wu, E. X.; Xu, B. *J. Am. Chem. Soc.* **2008**, *130*, 11828–11833.
(5) Su, C. H.; Sheu, H. S.; Lin, C. Y.; Huang, C. C.; Lo, Y. W.; Pu, Y. C.; Weng, J. C.; Shieh, D. B.; Chen, J. H.; Yeh, C. S. *J. Am. Chem. Soc.* **2007**, *129*, 2139–2146.
(6) Couvreur, P.; Vauthier, C. *Pharm. Res.* **2006**, *23*, 1417–1450.
(7) Nikitenko, S. I.; Koltypin, Y.; Palchik, O.; Felner, I.; Xu, X. N.; Gedanken, A. *Angew. Chem., Int. Ed.* **2001**, *40*, 4447–+.
(8) Dong, X. L.; Zhang, Z. D.; Jin, S. R.; Kim, B. K. *J. Appl. Phys.* **1999**, *86*, 6701–6706.
(9) Carpenter, E. E.; Calvin, S.; Stroud, R. M.; Harris, V. G. *Chem. Mater.* **2003**, *15*, 3245–3246.
(10) Seo, W. S.; Lee, J. H.; Sun, X. M.; Suzuki, Y.; Mann, D.; Liu, Z.; Terashima, M.; Yang, P. C.; McConnell, M. V.; Nishimura, D. G.; Dai, H. J. *Nat. Mater.* **2006**, *5*, 971–976.
(11) Ito, A.; Shinkai, M.; Honda, H.; Kobayashi, T. *J. Biosci. Bioeng.* **2005**, *100*, 1–11.
(12) Kohler, N.; Fryxell, G. E.; Zhang, M. Q. *J. Am. Chem. Soc.* **2004**, *126*, 7206–7211.
(13) Cheng, F. Y.; Su, C. H.; Yang, Y. S.; Yeh, C. S.; Tsai, C. Y.; Wu, C. L.; Wu, M. T.; Shieh, D. B. *Biomaterials* **2005**, *26*, 729–738.
(14) Burke, N. A. D.; Stover, H. D. H.; Dawson, F. P. *Chem. Mater.* **2002**, *14*, 4752–4761.
(15) Jana, N. R.; Earhart, C.; Ying, J. Y. *Chem. Mater.* **2007**, *19*, 5074–5082.
(16) Lyon, J. L.; Fleming, D. A.; Stone, M. B.; Schiffer, P.; Williams, M. E. *Nano Lett.* **2004**, *4*, 719–723.
(17) Ji, T. H.; Lirtsman, V. G.; Avny, Y.; Davidov, D. *Adv. Mater.* **2001**, *13*, 1253–1256.
(18) Kuhn, L. T.; Bojesen, A.; Timmermann, L.; Nielsen, M. M.; Morup, S. *J. Phys.: Condens. Matter* **2002**, *14*, 13551–13567.
(19) Grass, R. N.; Athanassiou, E. K.; Stark, W. J. *Angew. Chem., Int. Ed.* **2007**, *46*, 4909–4912.

Published on Web 06/09/2009

that these coatings may not only act as protection for the chemically highly active metal core from oxidative degradation and acid erosion, but may also be used for further surface functionalization with, for example, other nanoparticles or various ligands, depending on the respective application.

Polymer-coated metal nanoparticles are not stable at elevated temperatures and in contact with organic solvents (swelling, dissolution) because the intrinsically low stability of the polymer is often adversely affected by the catalytic activity of the nanoparticle's core itself.[20] This mostly restricts applications to biologically buffered aqueous systems as used in diagnostics. Silica coatings have enabled numerous fascinating applications;[15,21−24] however, it is challenging to obtain fully dense, nonporous silica shells.[20] As a consequence, the silica shell restructures under harsh environments (high or low pH conditions) which directly affects stability. Although the preparation of dense silica layers is difficult by classical coating methods, atomic layer deposition (ALD) recently enabled the preparation of nonporous SiO_2 on TiO_2 through subsequent deposition of silica onto titania particles.[25] The resulting silica-coated submicrometer-sized particles exhibited superior acid resistance both initially and over an extended time period. Covalent bonds to silica and other metal oxides, however, are prone to hydrolysis and make reliable attachment of ligands a challenge. Most recently, carbon-protected magnetic nanoparticles have received increasing attention.[26,27] Carbon cages have significant advantages such as remarkably high chemical and thermal stability as well as biocompatibility.[20]

Grass et al. have most recently reported the preparation of highly stable, nonagglomerated carbon-coated cobalt nanomagnets with excellent saturation magnetization synthesized in a scalable one-step flame spray synthesis process.[19] The carbon shell could be covalently surface-functionalized with *p*-chloro-, *p*-amino-, and *p*-carboxylphenylene units by a covalent bonding of the respective phenylene to the outermost carbon layer surrounding the nanomagnet. The C−C bond connecting the respective phenylene linker to the nanomagnet is significantly more stable in harsh environments (pH 0−14, solvents, $T_{\text{decompostition}} > 240$ °C) than, e.g., silanol bonds.[19] These (phenylenic) surface functionalities therefore provide a powerful linkage where organic molecules, such as catalytically active species,[28] drugs, or chelating agents, can be covalently attached to nanomagnets. These rapidly growing applications of functionalizable nanomagnets draw more and more attention to the need for a cost-effective, large-scale synthesis method for these nanomagnets. There, iron-based magnetic cores are of particular interest as they become more economical at larger scale.

In this work, we investigate the production of a palette of iron-based nanoparticles ranging from iron oxide (Fe_3O_4) to metallic iron (Fe) and iron carbide (Fe_3C), by one and the same method with only slight process modifications. In comparison to other techniques, e.g., wet phase or chemical vapor deposition (CVD), the herein described reducing flame spray synthesis process allows a dry, continuous, and scalable synthesis.[29,30] The process is based on industrially well-established flame aerosol processes that nowadays yield several megatons of silica, titania, and carbon black, annually. We demonstrate how the flame spray process can be modified to operate under inert atmosphere and oxygen limitation to enable the continuous production of carbon-encapsulated cementite nanomagnets of a high quality.[19,31] We further modified the surfaces of the magnetic nanoparticles by covalently functionalizing them with a range of linkers.

Experimental Section

Materials. For the preparation of iron nanoparticles, an air and humidity stable precursor was prepared by dissolving 284 g (5 mol) of metallic carbonyl iron (Sigma Aldrich, Fe ≥ 97%, mean particle size 4.5−5.2 μm) in 5 L of 2-ethylhexanoic acid (Sigma Aldrich, purum) through heating the mixture at 140 °C for 24 h. The resulting Fe(III)-2-ethylhexanoate with an iron content of 5 wt % was diluted 2:1 (w/w) with tetrahydrofurane (THF) (Fluka, technical grade) and filtered prior to use.

Flame Spray Synthesis of Iron Nanoparticles. The filtered iron precursor was fed at a flow rate of 6 mL min^{-1} (HNP Mikrosysteme, micro annular gear pump mzr-2900) into a spray nozzle, dispersed by oxygen (5 L min^{-1}, PanGas tech.), and ignited by a premixed methane−oxygen flame (CH_4, 1.2 L min^{-1}; O_2, 2.2 L min^{-1}; PanGas tech.) (see the Supporting Information for schematic representation of the setup). The combustion-generated particles were separated from the off-gas using glass fiber filters (Schleicher & Schuell, GF6). This procedure is well-known from the conventional flame spray synthesis. In the case of reducing flame spray synthesis, the spray nozzle was placed in a glovebox with a nitrogen atmosphere, which was continuously purged with nitrogen, and connected to a mass spectrometer for the online monitoring of hydrogen, oxygen, water, and methane concentrations, respectively.[31] During all syntheses, the oxygen content was kept well below 100 ppm (v/v). A sinter metal tube (GKN Sintermetalle, inner diameter 25 mm) surrounding the flame allowed radial inflow of N_2 (PanGas) at a flow rate of 25 L min^{-1}. Furthermore, acetylene (Pangas) could optionally be added at a well-defined flow-rate through the side walls of the tube. The addition of acetylene to the flame allows the

(20) Lu, A. H.; Salabas, E. L.; Schuth, F. *Angew. Chem., Int. Ed.* **2007**, *46*, 1222–1244.
(21) Bradley, C. A.; Yuhas, B. D.; McMurdo, M. J.; Tilley, T. D. *Chem. Mater.* **2009**, *21*, 174–185.
(22) Wu, T.; Zhang, Y. F.; Wang, X. F.; Liu, S. Y. *Chem. Mater.* **2008**, *20*, 101–109.
(23) Ma, D. L.; Guan, J. W.; Normandin, F.; Denommee, S.; Enright, G.; Veres, T.; Simard, B. *Chem. Mater.* **2006**, *18*, 1920–1927.
(24) Gerion, D.; Pinaud, F.; Williams, S. C.; Parak, W. J.; Zanchet, D.; Weiss, S.; Alivisatos, A. P. *J. Phys. Chem. B* **2001**, *105*, 8861–8871.
(25) King, D. M.; Liang, X. H.; Burton, B. B.; Akhtar, M. K.; Weimer, A. W. *Nanotechnology* **2008**, *19*, 8.
(26) Caiulo, N.; Yu, C. H.; Yu, K. M. K.; Lo, C. C. H.; Oduro, W.; Thiebaut, B.; Bishop, P.; Tsang, S. C. *Adv. Funct. Mater.* **2007**, *17*, 1392–1396.
(27) Wang, Z. F.; Mao, P. F.; He, N. Y. *Carbon* **2006**, *44*, 3277–3284.
(28) Hu, A. G.; Yee, G. T.; Lin, W. B. *J. Am. Chem. Soc.* **2005**, *127*, 12486–12487.
(29) Grass, R. N.; Stark, W. J. *J. Nanopart. Res.* **2006**, *8*, 729–736.
(30) Grass, R. N.; Stark, W. J. *J. Mater. Chem.* **2006**, *16*, 1825–1830.
(31) Athanassiou, E. K.; Grass, R. N.; Stark, W. J. *Nanotechnology* **2006**, *17*, 1668–1673.

production of carbon-encapsulated particles, as described earlier by Athanassiou et al.[32]

Because no additional oxygen is provided from the nitrogen atmosphere in the glovebox, the overall content of oxygen entering the flame is predefined by the operating conditions (oxygen flow to the flame). The degree of oxidation in the flame process may therefore be characterized by the fuel to oxygen ratio ϕ, which is defined as

$$\phi = \frac{\text{moles of } O_2 \text{ required for complete combustion}}{\text{moles of } O_2 \text{ available}}$$

Particle Characterization. The as prepared nanoparticles were analyzed by means of X-ray diffraction (Siemens powder X-ray diffractometer with Ni-filtered CuKα radiation, step size 0.3°) for crystallinity and predominant phase composition, transmission electron microscopy (CM30 ST-Philips, LaB_6 cathode, operated at 300 kV, point resolution $\approx$ 4 Å), scanning electron microscopy (LEO 1530 Gemini, Accelerating voltage 10 kV), magnetic hysteresis susceptibility (vibrating sample magnetometer, VSM, Princeton Measurements Corporation, model 3900), and thermal gravimetric analysis (Linseis TG/STA-PT1600 theromanalyzer, temperature range 25−700 °C, heating rate 10 °C min^{-1}, air). The chemical identity of all materials was confirmed using IR spectroscopy. Fourier transform IR (FTIR) measurements of particle samples were done in KBr pills (5 wt % particles) using a Tensor 27 Spectrometer (Bruker Optics, equipped with a diffuse reflectance accessory, DiffusIR, Pike technologies). As-prepared C/Fe_3C nanoparticles were taken as a background to improve the spectrum quality. The carbon, hydrogen, and nitrogen contents were determined by microanalysis (LECO, CHN-900). Nitrogen adsorption was performed on a Tristar (Micromeritics Instruments) after sample pretreatment under a vacuum at 150 °C for 1 h. The chemical stability of the carbon-encaged nanoparticles was investigated by stirring 10 g of particles in 1350 mL of 24 v% hydrochloric acid for 7 days. The hydrochloric acid solution was exchanged every 24 h. After 1 week, the nanoparticles were removed from the suspension by magnetic separation, washed three times with water and acetone, respectively, and dried under a vacuum at 60 °C overnight. The oven-dry mass was determined afterward.

Covalent Surface Functionalization. Carbon-coated iron carbide particles were surface-functionalized by radical chemistry (diazotation) following a procedure initially described by Grass et al. for carbon-coated cobalt particles.[19] The carbon-coated magnetic nanoparticles were derivatized using 4-nitrobenzenediazonium tetrafluoroborate salt, following a well-established procedure previously applied for the functionalization of carbon nanotubes[33−35] and graphene.[36] Alternatively, the carbon surface was functionalized in a single-step reaction with a sulfonic acid or an alkylamine functionality by reaction with the respective aniline derivates (see Figure 5). After each synthesis step, the nanoparticles were extensively washed with the solvents hexane, water, and acetone three times each in order to remove unreacted substrates. To demonstrate that the surface functionalities on the particles could be further used for reaction sequences, 2-phenyl ethyl amine functionalized nanomagnets were reacted with palmitinic acid chloride to form an amide bond and thus covalently bind the palmitoyl group. Again, the particles were washed following the above-mentioned procedure ensuring the complete removal of unreacted species. Palmitinic acid was chosen as a simple model carboxylic acid in order to monitor the amide bond formation by IR-spectroscopy. This test reaction can be viewed as an example that can be extended to more complex substrates and reactions.

Results and Discussion

From Iron Oxide to Iron, and Iron Carbide. Combustion of iron-2-ethylhexanoate in a conventional flame spray synthesis setup allows the production of iron oxides at a production rate of 15 g h^{-1}. If the flame spray nozzle is moved into a reducing environment, oxygen becomes the limiting species and the combustion of the iron precursor produces lightweight black metallic nanopowders, as shown earlier by Grass et al. for cobalt[30] and Athanassiou et al. for NiMo alloys.[37] In contrast to classical flames where the fuel limits the combustion process and oxygen is plentiful through the surrounding air, the here-used setup consists of an oxygen limited flame. The above-described reducing flame spray synthesis setup enables a continuous production of iron-based nanoparticles with a carbon content varying between 1.8 and 8.05 wt %, depending on the acetylene flow rate (see Figure S1 in the Supporting Information).

In contrast to copper and cobalt, iron has a most complex Fe/C phase diagram and numerous intermetallic carbon−iron phases yield various degrees of technically useful metals or oven steels. By systematically altering the flame feed composition, we therefore followed the subsequent reduction of iron oxide to iron and iron carbides, as schematically depicted in simplified Fe/O and Fe/C phase diagrams (Figure 1). Using a slightly reducing flame (ϕ = 2) allowed preparation of metallic iron nanoparticles as a black powder at a production rate of 10 g h^{-1}. X-ray diffraction (Figure 2) and electron microscopy (Figure S2 in the Supporting Information) confirmed the formation of 20−50 nm sized particles of metallic α-iron. The powder can be partially passivated through an oxide surface layer (see Figure S2 in the Supporting Information). It spontaneously ignites if rapidly removed from the protective atmosphere (N_2, H_2) without prior passivation.

To make iron nanoparticles more useful for technical applications, we investigated the in situ one-step deposition of protective carbon layers on top of the iron metal particles. Adding acetylene to a reducing flame, we obtained a fully air stable lightweight black powder with exceptionally high saturation magnetization. In agreement with the iron−carbon phase diagram, the metallic iron core took up about 6.7 wt % C (corresponds to Fe_3C, cementite) as confirmed by XRD, by

(32) Athanassiou, E. K.; Mensing, C.; Stark, W. J. *Sens. Actuators, A* **2007**, *138*, 120–129.
(33) Hirsch, A. *Angew. Chem., Int. Ed.* **2002**, *41*, 1853–1859.
(34) Strano, M. S.; Dyke, C. A.; Usrey, M. L.; Barone, P. W.; Allen, M. J.; Shan, H. W.; Kittrell, C.; Hauge, R. H.; Tour, J. M.; Smalley, R. E. *Science* **2003**, *301*, 1519–1522.
(35) Dyke, C. A.; Tour, J. M. *Nano Lett.* **2003**, *3*, 1215–1218.
(36) Koehler, F. M.; Luechinger, N. A.; Ziegler, D.; Athanassiou, E. K.; Grass, R. N.; Rossi, A.; Hierold, C.; Stemmer, A.; Stark, W. J. *Angew. Chem., Int. Ed.* **2009**, *48*, 224–227.
(37) Athanassiou, E. K.; Grass, R. N.; Osterwalder, N.; Stark, W. J. *Chem. Mater.* **2007**, *19*, 4847–4854.

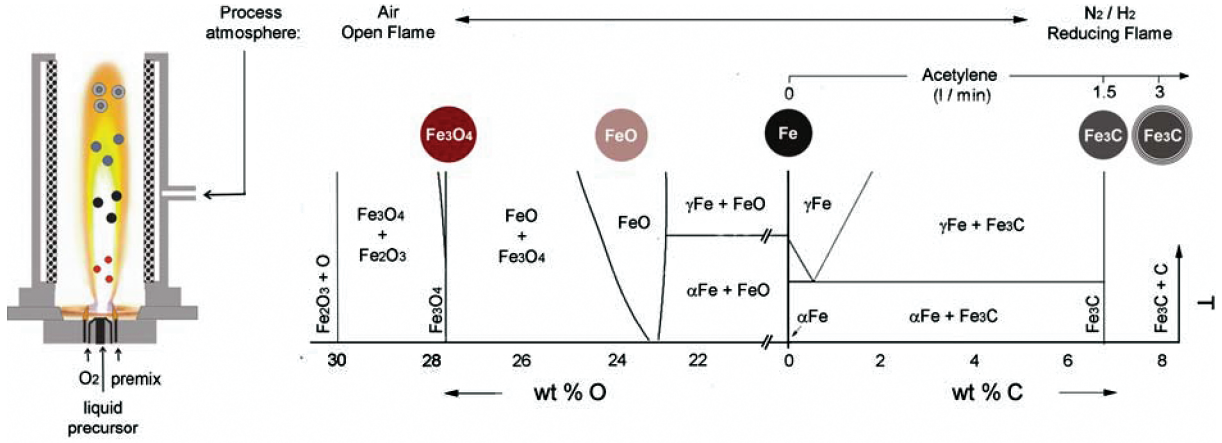

Figure 1. Controlling the process atmosphere during flame spray synthesis allows preparation of a wide variety of iron-based nanoparticles. The product composition stays in agreement with the corresponding phase diagrams for Fe/O (left side) for oxidizing conditions. Subsequent reduction yields iron and iron carbide nanoparticles as predicted through the Fe/C phase diagram (right).

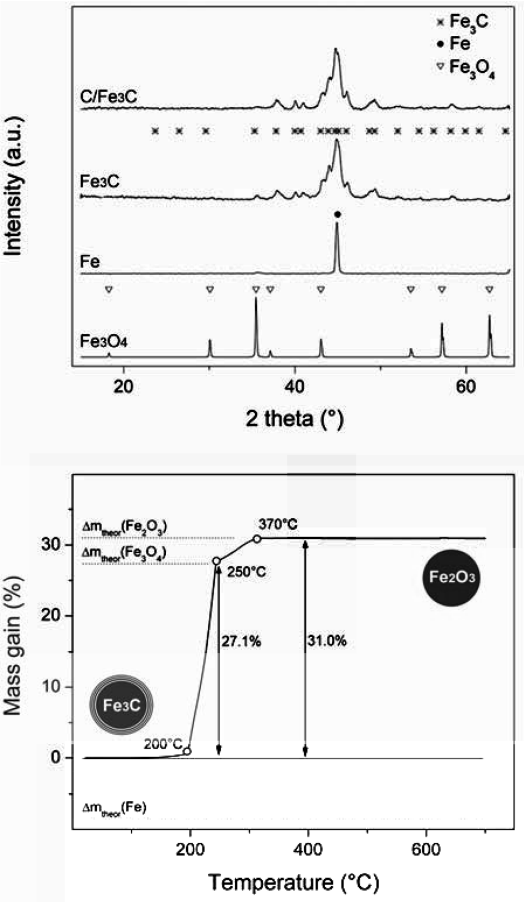

Figure 2. X-ray diffraction patterns of as-prepared iron oxide, iron, iron carbide, and carbon-coated iron carbide nanoparticles (*, Fe_3C; ●, Fe; ▽, Fe_3O_4) (top). Quantitative analysis of iron and oxide content in C/Fe_3C nanoparticles (bottom). The powder mass gain upon oxidation measured by thermogravimetry in air of as-prepared carbon-coated iron carbide nanoparticles shows two mass steps corresponding to the partial oxidation to Fe_3O_4 ($T \approx 200$ °C) and the subsequent total oxidation to Fe_2O_3 ($T \approx 250$ °C), respectively.

microanalysis, and TEM (see Figure S3 in the Supporting Information). An additional carbon coating of a few graphene layers can be found on the nanoparticles from a flame with high acetylene feed (≥3 L min^{-1}) (8.05 wt % C).

The iron-based nanoparticles produced in the classical flame spray synthesis process and the particles produced in the reducing flame spray syntheses with acetylene addition were air stable. The powder synthesized under reducing atmosphere without adding acetylene, however, ignited immediately upon contact with air. Because high stability, high magnetization, and a surface that can be covalently functionalized are absolutely crucial prerequisites for the initially mentioned industrial applications, emphasis is hence put on the stable, carbon-coated particles.

Crystal Phase Composition. X-ray diffractions of the nanoparticles produced under an inert atmosphere shows that the conversion has produced bare metallic iron nanoparticles (Figure 2). The X-ray diffraction pattern of the air-stable samples produced under a nitrogen atmosphere showed the formation of cementite (Fe_3C) and complete absence of crystalline iron oxide species (Figure 2). Additionally, X-ray diffractions of magnetite (Fe_3O_4) nanoparticles produced in a classical flame spray synthesis process under ambient conditions are included in Figure 2. This shows that the whole palette from reduced iron carbide phase (Fe_3C) and iron (Fe) to iron oxides (Fe_3O_4) is accessible by a single process with only slight process modifications (see Figure 1).

Morphology, Topology, and Particle Size Distribution. Examination of the as-prepared iron carbide samples by transmission electron microscopy (TEM) confirms that the conversions have produced bare iron-carbide nanoparticles and iron carbide nanoparticles encapsulated by spherical graphite cages of 3−5 graphene-like sheets for an acetylene flow rate of 1.5 and 3 L min^{-1}, respectively (see Figure S3 in the Supporting Information and Figure 3B). This shows that the layer thickness of the carbon coating can be controlled to a certain extent by the flow rate of acetylene added to the flame.

Scanning electron microscopy (SEM) images were used to determine the mean diameter of the as-prepared carbon-coated iron carbide particles (Figure 3A). The particles were found to have mean diameter of 30 nm and a narrow size distribution with a geometric standard

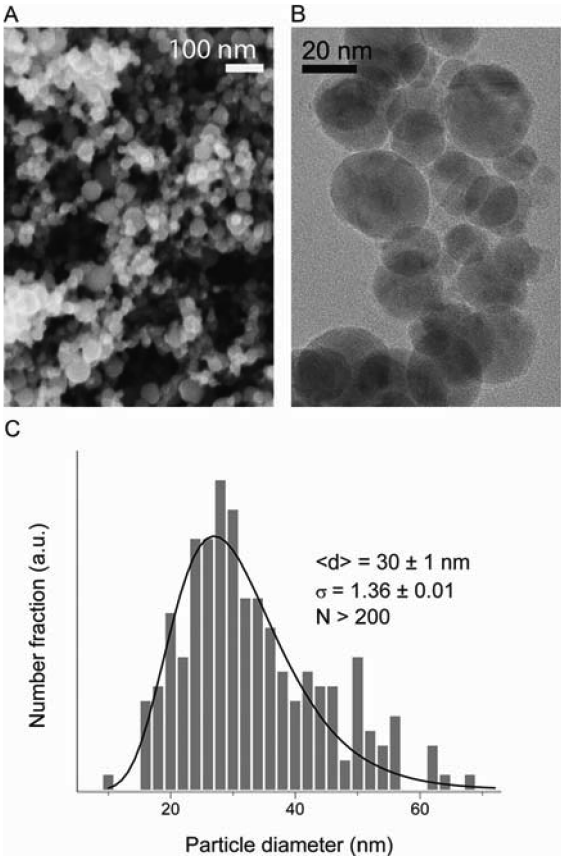

Figure 3. (A) Scanning electron microscopy (SEM) and (B) transmission electron microscopy (TEM) images of the as-prepared carbon-encapsulated cementite nanomagnets and (C) full particle size distribution. The absence of large particles and a smooth, log-normal size distribution confirm the preparation of well-characterized samples of nanomagnets.

deviation $\sigma_{g,n}$ of 1.36 (Figure 3C). The log-normal shape of the particle size distribution as well as the number based geometric standard deviation $\sigma_{g,n}$ are in close agreement with modeling results based on Brownian aggregation for nanoparticles in the gas phase (theoretical value of $\sigma_{g,n}$ is 1.46, spheres, free molecular regime).[38] This log-normal shape of the particles size distribution also shows the readily identifiable similarity of the process to the well-established industrially applied flame spray process. Although the absence of hard agglomerates (particles sintered together or covalently bound through connected carbon layers) can not be entirely excluded at present; earlier detailed studies[39,40] on particles derived from similar flames did not show pronounced formation of hard agglomerates (consisting of 1−30 primary particles). Information on the hydrodynamic diameter of the carbon-coated iron carbide nanomagnets can be found in Figure S4 of the Supporting Information. Nitrogen adsorption at −196 °C according to Brunauer−Emmett−Teller (BET) yielded a surface area of 30.5 $m^2 g^{-1}$ or a calculated surface area equivalent primary particle size d_{BET} 25 nm.

Thermal and Chemical Stability. The thermal stability and oxygen uptake of the carbon-coated iron carbide nanoparticles were measured in a thermobalance. The mass profile showed that the carbon-coated iron carbide nanopowder was perfectly stable under air up to 200 °C, where it ignited (mass gain of about 27.1%, corresponding to the partial oxidation of C/Fe_3C (8.05 wt % C) to Fe_3O_4, with a theoretical mass gain of 27%) followed by a slow oxidation to a total mass gain of 31.0% (conversion of Fe_3O_4 to Fe_2O_3) (Figures 2 and Figure S5 in the Supporting Information). Comparison of the experimental (thermogravimetric) data and the calculated total mass gain of 31.5% (assuming full oxidation to Fe_2O_3) confirmed that the iron in the here presented materials is nonoxidic which further fully agrees with the XRD analysis (Figure 2).

The chemical stability was investigated by stirring the as-prepared carbon-coated iron carbide nanoparticles for 7 days in 24% (v) aqueous hydrochloric acid (pH ≪1). By subsequent magnetic separation, about 80 wt % of the particles could be successfully recovered. X-ray diffraction tests confirmed that no phase transitions occurred during this harsh washing procedure. Thus it can be assumed that 80 wt % of the as-prepared particles are entirely coated by protective graphene-like shells and therefore resistant against harsh conditions (pH ≪1) for more than a full week. This stays in sharp contrast to, e.g., magnetite, which readily dissolves under (strongly) acidic conditions within seconds as shown by Sidhu et al.[41]

Magnetic Properties. Figure 4 shows the magnetic hysteresis loop of the as-prepared carbon-coated iron carbide recorded at 298 K. The hysteresis loop showed a relatively small coercivity of 250 Oe, together with a high saturation magnetization of 140 emu g^{-1}. At room temperature, the magnetization shows a tendency to saturate at a field strength of 7.5 kOe. The shape of the hysteresis loop suggests that the contribution of superparamagnetic particles on the hysteresis curve is negligible. The experimentally determined saturation magnetization value of the as-prepared carbon-coated cementite nanoparticles is in good agreement with the value of bulk cementite (140 emu g^{-1}).[42] A reduction of the nanoparticles' saturation magnetization due to the formation of a surface shell with spin disorder, as described by Sajitha et al.,[42] has not been observed in this case.

We further demonstrated that the magnetic nanoparticles can be easily recovered from suspensions by applying a magnetic field induced by a 1 cm^3 cubic neodymium permanent magnet placed next to the vial (see Figure 4B). The high saturation magnetization and the fast and complete recovery of the particles by magnetic separation suggest that the carbon encapsulation successfully

(38) Dekkers, P. J.; Friedlander, S. K. *J. Colloid Interface Sci.* **2002**, *248*, 295–305.
(39) Brunner, T. J.; Wick, P.; Manser, P.; Spohn, P.; Grass, R. N.; Limbach, L. K.; Bruinink, A.; Stark, W. J. *Environ. Sci. Technol.* **2006**, *40*, 4374–4381.
(40) Limbach, L. K.; Li, Y. C.; Grass, R. N.; Brunner, T. J.; Hintermann, M. A.; Muller, M.; Gunther, D.; Stark, W. J. *Environ. Sci. Technol.* **2005**, *39*, 9370–9376.
(41) Sidhu, P. S.; Gilkes, R. J.; Cornell, R. M.; Posner, A. M.; Quirk, J. P. *Clays Clay Miner.* **1981**, *29*, 269–276.
(42) Sajitha, E. P.; Prasad, V.; Subramanyam, S. V.; Mishra, A. K.; Sarkar, S.; Bansal, C. *J. Phys.: Condens. Matter* **2007**, *19*, 13.

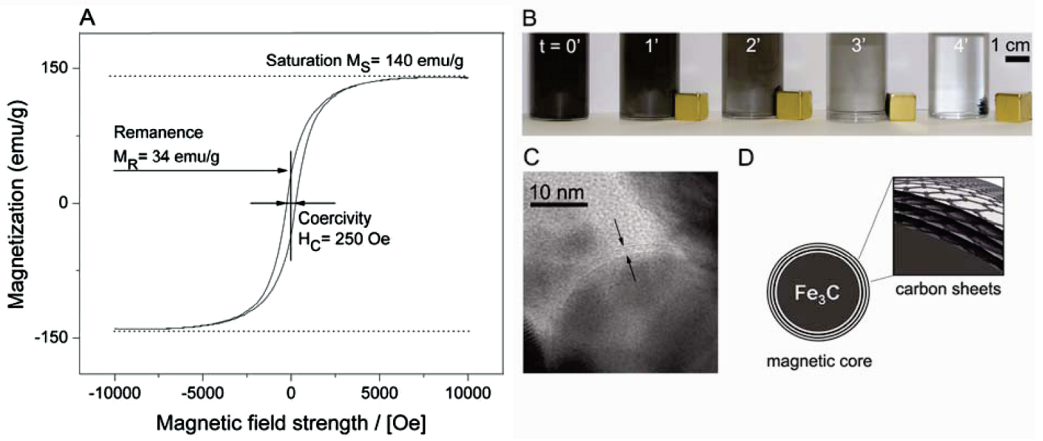

Figure 4. (A) Magnetic hysteresis curve of carbon-coated iron carbide nanoparticles at room temperature. (B) Fast and complete recovery of nanomagnets from suspension within 4 min. (C) Electron micrograph (TEM) displaying core−shell-type structure of cementite nanomagnets, and (D) schematic representation of the magnetic cementite core with the protective carbon shell.

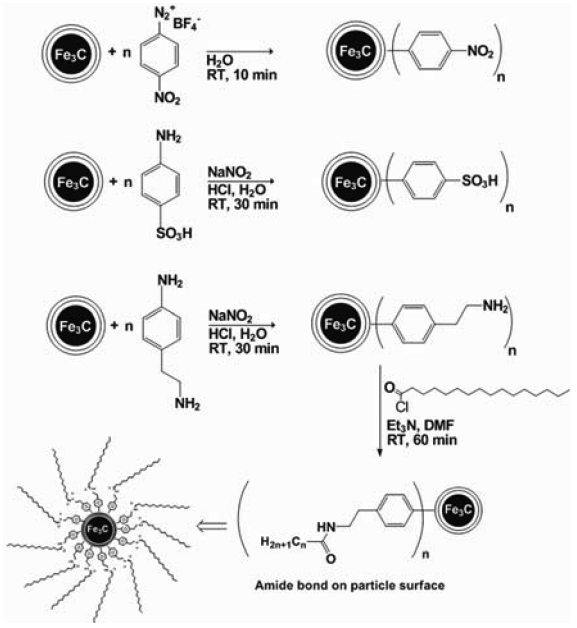

Figure 5. Functionalization of carbon-coated nanomagnets with nitrobenzene, benzenesulfonic acid, and benzyl alkyl amine, respectively. The reaction of amine-functionalized nanomagnets with palmitinic acid chloride is illustrated as a model reaction for further derivatization of the nanomagnets (bottom scheme).

protects the magnetic core form oxidation and subsequent loss of magnetism. Panels C and D in Figure 4 show a transmission electron microscopy image and the corresponding scheme of how the magnetic core is protected by the carbon shell.

Covalent Surface Functionalization. To meet the initially mentioned requirements for nanomagnets of broad application, the covalent surface functionalization is a key issue and allows us to tailor the surface of the magnets according to a given application. The possibility to attach organic molecules to a nanomagnet can be realized only through a highly stable connection between the magnet surface and a reactive linker group (Figure 5). Additionally, the number of these linker funtionalities on the surface is crucial for a good loading (density of surface molecules per mass of magnets) and large capactity for further functionalization.[20] To characterize the functionalized nanomagnets, before and after functionalization, IR spectroscopy was used for the identification of the functional groups.[19] The binding capacity was calculated from quantitative CHN microanalysis through directly measuring the mass of the attached molecules. The IR spectra of the surface-functionalized nanomagnets are shown in Figure 6. The comparison with the corresponding reference components confirms the presence of nitro- and sulfonic acid groups on the particle surface. The surface loading was calculated from the CHN data to be 0.3 mmol/g for nitro-benzene and 0.1 mmol/g for benzenesulfonic acid. The sulfonic acid group loading was further verified by titration of the acidic groups following the procedure described by Gill et al.[43] Again, a loading of 0.1 mmol acid sites/g nanoparticles was found, which is in good agreement with the microanalysis data.

The model test reaction between alkylamine-benzyl functionalized nanomagnets (0.11 mmol per gram) and a carboxylic acid chloride (palmitoyl chloride) proved to be successful (Figure 5). Amide bonds can be identified in the IR spectra shown in Figure 6. The capacity of palmitinic amide on the surface of the particles could be calculated from the microanalysis data to be 0.09 mmol per g of nanoparticles, which corresponds to an approximate reaction yield of 80% based on the loading of amine functionalities on the particles. This shows that the nanomagnets' surface functionalities are amenable to further derivatization.

Cost-Efficient, Large-Scale Production. Similar to an oil lamp producing soot continuously under low oxygen conditions, flame spray pyrolysis produces metallic nanoparticles of different composition by burning the respective 2-ethylhexanoic acid-based metal precursor. The herein described process has substantial similarity to the well-established industrial flame spray pyrolysis process, making it particularly suitable for large-scale productions of nanoparticles. Grass and Athanassiou[19,30,37] recently demonstrated how suitable modifications of the

(43) Gill, C. S.; Price, B. A.; Jones, C. W. *J. Catal.* **2007**, *251*, 145–152.

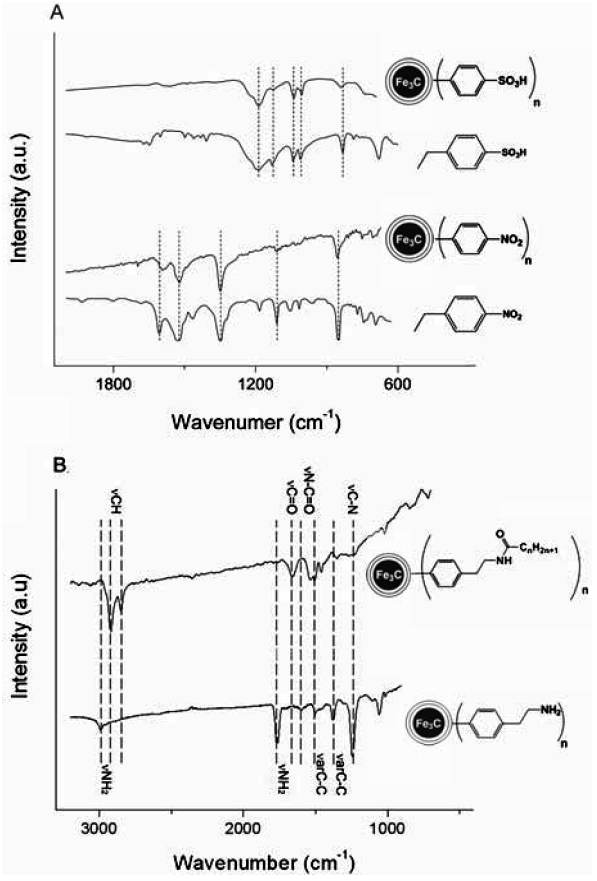

Figure 6. (A) Infrared spectra of C/Fe_3C powder after reaction with 4-nitrobenzenediazonium salt (second trace from the bottom) and with the corresponding sulfonic acid (top trace), respectively; reference spectra of 4-ethyl-benzyl sulfonic acid (second trace from the top) and 4-ethylnitrobenzene (bottom trace). (B) IR spectra of the alkyl amine functionalized nanoparticles before and after reaction with palmitinic acid chloride. The characteristic bands of an amide bond can be recognized in the top trace.

conventional flame process has given access to the preparation of a much broader range of products, including bismuth, cobalt, copper and even metal alloy nanoparticles. From an economic and environmental perspective, iron-based nanomagnets become much more interesting at larger scales (see Figure S6 in the Supporting Information). Additionally, iron nanoparticles are more attractive for use in biological systems and if contacted with humans or environment in, e.g., open processing or application areas. Although cobalt is an essential micrometerutrient as a cofactor of vitamin B_{12}, inorganic cobalt is associated with various human diseases such as lung cancer and asthma, among others.[44] With growing applications for nanomagnets, the impact on the environment will grow continuously. The above-described nanomagnets offer an attractive choice because they consist only of iron and carbon, which are believed to be nontoxic. Detailed studies on the toxicity of the nanomagnets, however, are still needed.

(44) Stadler, J. A.; Schweyen, R. J. *J. Biol. Chem.* **2002**, *277*, 39649–39654.

Conclusion

In this work, we have demonstrated that iron-based core−shell nanomagnets with a very high saturation magnetization (140 emu g^{-1}) can be synthesized in a continuous one-step low-cost process at a production rate exceeding 10 g h^{-1} even at laboratory scale. The obtained nanoparticles proved to be thermally stable up to temperatures of 200 °C and the recovery of about 80 wt % of the initial weight after curing the as-prepared nanoparticles for 1 week in strongly acidic (pH $\ll$1) solutions attests to their high quality. The high stability of these core−shell nanomagnets suggests that the 3−5 graphene sheet layered carbon cage successfully protects the inner magnetic metal core from oxidation and subsequent loss of magnetism. It is shown that the carbon encapsulation of these core−shell nanomagnets serves not only as protection layer but enables a C−C bond-based covalent surface functionalization withstanding harsh environmental conditions. Here, we demonstrate that the surface functionalities can be further reacted, obtaining comparatively high surface loadings of up to 0.1 mmol functionalities per g of nanomagnets.

It is noteworthy that these highly stable core−shell nanomagnets consist exclusively of nontoxic elements. This makes them particularly attractive for biotechnological and medicinal applications.

We demonstrated how classical high-temperature chemistry could be translated in an aerosol process, thus providing a fascinating array of stable nanomagnets.

Acknowledgment. The authors acknowledge financial support by ETH Zurich in the form of a TH Grant (TH-02 07-3) and the Swiss National Science Foundation (SNF 200021-116123).

Supporting Information Available: Experimental setup (Figure S1), transmission electron micrographs (TEM) of flame-made α-iron nanoparticles (Figure S2) and bare cementite nanoparticles (Figure S3), hydrodynamic diameter of carbon-coated iron carbide nanomagnets (Figure S4), subsequent oxidation steps observed in TGA (Scheme S5), cost calculation for magnetic materials (Scheme S6) (PDF). This material is available free of charge via the Internet at http://pubs.acs.org.